

One-carbon chemistry of oxalate oxidoreductase captured by X-ray crystallography

Supporting Information – Materials and Methods

Protein Purification

OOR was purified from *M. thermoacetica* by the methods described (1), concentrated to 45 mg/ml, as determined by the rose bengal method (2) with a lysozyme standard and was stored in a storage buffer of 50 mM Tris pH 8.0 and 2 mM dithiothreitol under an anoxic nitrogen atmosphere. OOR was determined to have an activity of 0.032 U/mg at 25 °C in standard assay conditions of 50 mM Tris-HCl, pH 8.2 and 10 mM methyl viologen, which is comparable to that previously reported (1). Aliquots of 200 to 500 μ L were flash-frozen in liquid nitrogen for long-term storage in liquid nitrogen.

Crystallization

OOR was crystallized by the hanging drop vapor diffusion method at room temperature in a Coy anaerobic chamber under an Ar/H₂ gas mixture, as described previously (3). Briefly, 30 mg/ml OOR in the storage buffer (50 mM Tris pH 8.0 and 2 mM dithiothreitol) was mixed with the well solution (8-11% PEG 3,000, 3-4% Tacsimate, pH 7.0) in a 1:1 ratio to make a 2 μ l hanging drop with a final protein concentration of 15 mg/ml. Tetragonal crystals in the space group $P4_3$ grew in 2-4 days. One of these crystals was soaked for 2 minutes in a solution mimicking the mother liquor but with the addition of 100 mM oxalic acid (Sigma-Aldrich) solution, pH 8.0 (the pH was adjusted with 10 M NaOH), to a final concentration of 10 mM oxalic acid, 15% PEG 3,000, 2% Tacsimate pH 7.0, 25 mM Tris pH 8.0, 1 mM dithiothreitol, and 20% PEG 400, which served as a cryoprotectant. After soaking, the crystal was cryo-cooled in liquid nitrogen.

Oxalate co-crystals were grown in an anaerobic chamber in the same condition as described above, in drops composed of 1 μ l well solution and 1 μ l OOR (30 mg/ml), but with the addition of 0.2 μ L of 100 mM oxalic acid, pH 8.0 to the crystallization drop. Long, rod-like crystals grew in 2-4 days, in the space group $P2_12_12_1$ with unit cell constants $a = 113.6 \text{ \AA}$, $b =$

144.1 Å, $c = 161.7$ Å. One of these crystals was cryo-protected using PEG 400, in a solution containing: 20% PEG 400, 15% PEG 3,000, 2% Tacsimate pH 7.0, 25 mM Tris pH 8.0, and 1 mM dithiothreitol. Due to the fragility of the crystals, this cryosolution was added directly to the crystallization drop in two successive additions of 1 μ l and removal of 1 μ l from the opposite side of the drop, followed by a final addition of 2 μ l. The drop was allowed to equilibrate for 2 minutes after each addition. After the final addition, crystals were looped and cryo-cooled in liquid nitrogen.

Data Collection and Processing

Data were collected at the Advanced Photon Source on Northeastern Collaborative Access Team beamline 24-ID-C on a Pilatus 6MF detector. HKL 2000 (4) was used to process all of the datasets (see Supporting Table 1). Data for the oxalate-soaked crystal and the oxalate co-crystal extended to 2.50-Å and 1.88-Å resolution, respectively. The oxalate-soaked crystal was determined by Phenix Xtriage (5, 6) to have merohedral twinning, with a twin law of $h, -k, -l$. The twin fraction refined in Phenix Refine (7) to 35%, and the structure was refined to account for twinning.

Structure Determination and Refinement

The structure of OOR (3) was used as a search model for molecular replacement (MR) in each dataset, which was performed with Phenix (Phaser-MR) (8). MR was necessary for the determination of both structures because both crystals had different unit cells than the high resolution native structure, which crystallized in the space group $P2_12_12_1$ with unit cell constants $a = 84$ Å, $b = 152$ Å, and $c = 172$ Å. A search model with amino acid sidechains and cofactors and a resolution cutoff of 3.5 Å was used for the MR search in both instances. In the oxalate-soaked crystal, the asymmetric unit was found to contain two OOR dimers. In the oxalate co-crystal, the asymmetric unit contained one OOR dimer. Once a MR solution was found, one round of rigid-body refinement into the full-resolution dataset was performed to verify the placement of the molecules and improve the electron-density maps. Iterative rounds of model-

building in COOT (9) and refinement of atomic coordinates and *B*-factors in Phenix (7) allowed for the correct placement of sidechains and loops where they differed from the starting model. NCS restraints were used throughout refinement of the oxalate-soaked crystal. In each of the structures, potential covalent adducts to C2 of the TPP ligand were identified by positive difference density in the F_o-F_c maps. Adducts to TPP were allowed to refine to partial occupancy while holding *B*-factors constant.

Restraints for resting TPP were based on the crystal structure of a pyruvate decarboxylase (PDB 2VK8). Restraints for the COOM-TPP intermediate and the carboxy-TPP intermediate were generated from geometry optimization calculations in Gaussian 03 (10), using a B3LYP hybrid density functional (11–13) with a 6-311++G basis set for all atoms. For the calculations, TPP was trimmed down to 3,4,5-trimethyl-3 γ 4-thiazole. End-state frequency calculations were performed to ensure a minimum energy potential had been reached. An unrestricted functional was used for carboxy-thiazole calculations, so that all three oxidation states could be compared. The differences in calculated bond lengths and angles between reduced, 1-electron oxidized, and 2-electron oxidized CO₂-thiazole were small enough that they would be indistinguishable at the resolution of the crystal structures. The calculated bond distances and angles for the COOM- and carboxy-thiazole intermediates were used to update previously employed TPP restraints. The carboxy group was restrained to be planar with the thiazole ring, whereas the dihedral angle between oxalate and the thiazole ring was allowed a greater degree of freedom to account for specific interactions with the protein. Restraints for the iron-sulfur clusters were based on *Moorella thermoacetica* carbon monoxide dehydrogenase/acetyl-CoA synthase (PDB 3I01) (14), though they were loosened for the higher resolution structures.

In the structures from both the oxalate-soaked crystal and the oxalate co-crystal, residues 113-117 of chain α , which form a loop in the substrate-binding pocket, were disordered to some extent, with the electron density suggesting two distinct conformations. In the soaked crystal,

the data were sufficient to model one orientation for this loop. In the co-crystal, however, the higher resolution and clearer difference density made it possible to model this loop in two conformations. Protein regions that were modeled in two conformations are shown in Supporting Table 2.

Composite-omit electron density maps (made with Phenix Autobuild (7)) were used to validate the final models. For each dataset, residues not having sufficient electron density were omitted from the model or modeled as alanine. Model completeness along with omitted residues is shown in Supporting Table 2. Solvent water molecules were generated automatically and refined by Phenix using a sigma cutoff of 3.5. Prior to refinement, 5.0% of unique reflections from the each dataset were set aside as test datasets, from which Rfree values are calculated. Different test datasets were used for each structure due to the fact that each structure was determined in a different unit cell. Final refinement statistics are shown in Supporting Table 1.

OOR crystal activity assay

OOR crystals were grown as described above. A wash solution was prepared with 25 mM Tris pH 8.0, 1 mM DTT, 8% PEG 3,000, 1% Tacsimate. Crystals were looped under an anoxic atmosphere and washed sequentially in two 4- μ l drops of wash solution. Three 2- μ l experimental drops were prepared with a base of the wash solution, and additional reagents as follows: Drop 1 – four crystals with 10 mM methyl viologen (oxidized); Drop 2 – 10 mM oxalate, pH 8.0, 10 mM methyl viologen (oxidized) (no crystals); Drop 3 – four crystals with 10 mM oxalate, pH 8.0, 10 mM methyl viologen (oxidized). The first drop was a control for OOR oxidizing the crystallization solution; the second drop was a control for free oxalate reducing methyl viologen; the third drop tested whether crystallized OOR is active in the oxidation of oxalate, reducing methyl viologen and changing its color to blue. The sitting-drop plate that was used to hold the drops was sealed with the wash solution in the well to keep the drops from drying out. After 24 hours, the drops were observed for blue color, indicative of methyl viologen reduction.

Supporting Information - Figures

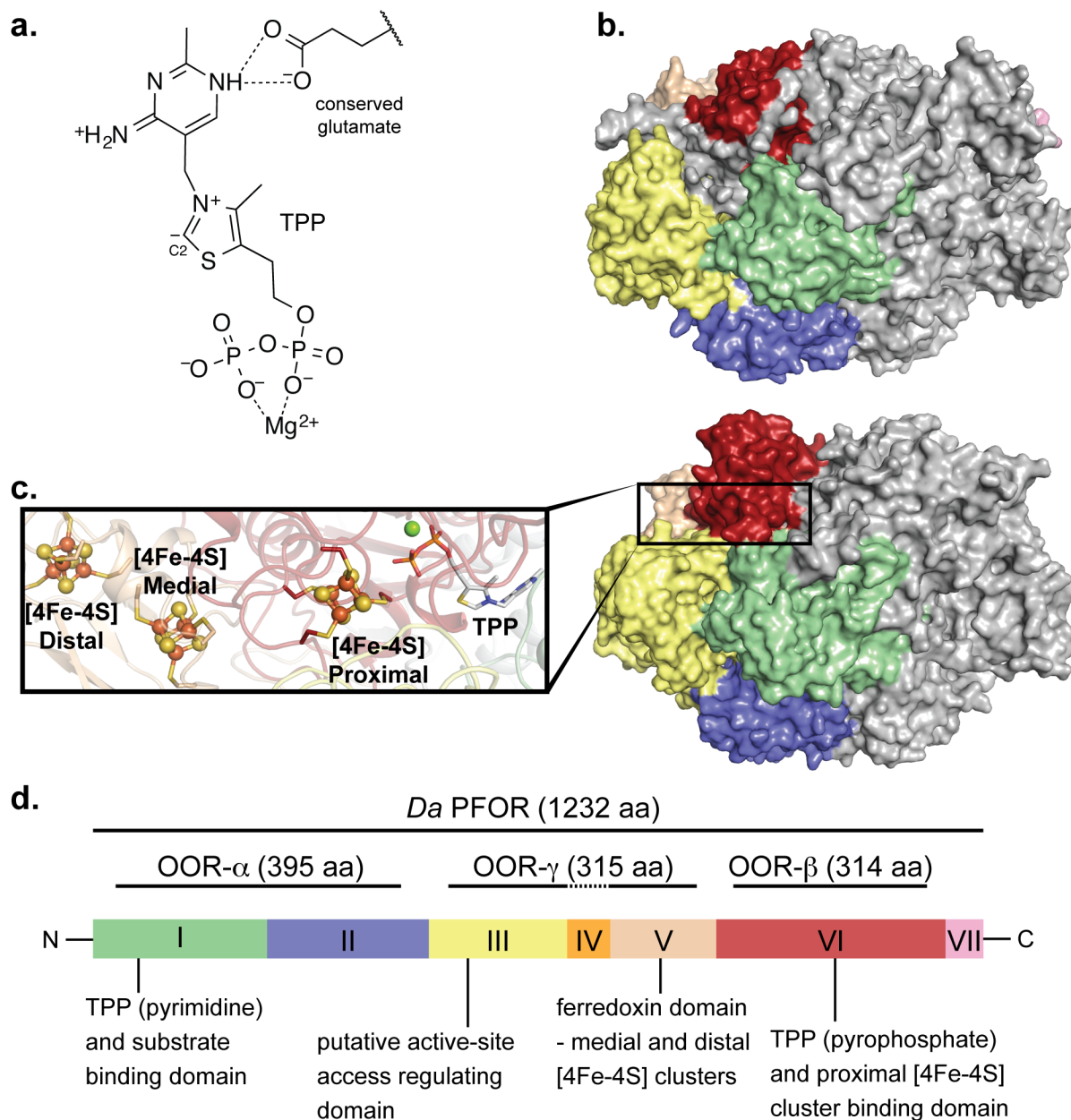


Figure S1. Features of 2-oxoacid:ferredoxin oxidoreductases. **a)** TPP is the catalytic cofactor in both OOR and PFOR. C2 of the thiazole ring is deprotonated by the imine group of the adjacent iminopyrimidine moiety, the tautomer of which is preferentially stabilized by a glutamate residue that is conserved across all TPP-utilizing enzymes. The pyrophosphate moiety of TPP coordinates a divalent cation such as Mg^{2+} or Ca^{2+} . **b)** The catalytic α_2 dimer of PFOR (PDB ID: 2C42) is shown in surface representation. The right monomer is colored gray, whereas the left monomer is colored by domain: I – green; II – blue; III – yellow; IV – orange (not visible); V – wheat; VI – red; VII – pink. **c)** The catalytic $(\alpha_1\beta)_2$ dimer of OOR (PDB ID: 5C4I) is shown as in b). The inset depicts the redox cofactors of the left monomer of OOR: the [4Fe-4S] clusters are

shown as ball-and-stick models, TPP is shown as white sticks, and the Mg^{2+} as a green sphere.

d) The domain arrangement of *Da* PFOR is shown as a series of colored boxes denoted by Roman numerals I – VII from N to C terminus. The black line across the top indicates that *Da* PFOR has all of these domains in a single 1232 residue peptide chain. The three black lines underneath labeled OOR- α , OOR- γ , and OOR- β indicate the domain composition of the three OOR chains that form the monomeric $\alpha\gamma\beta$ unit. The dashed line in the middle of OOR- γ indicates that OOR does not have a domain IV. Also missing from OOR is domain VII. The functions of domains I, III, V, and VI are labeled at the bottom.

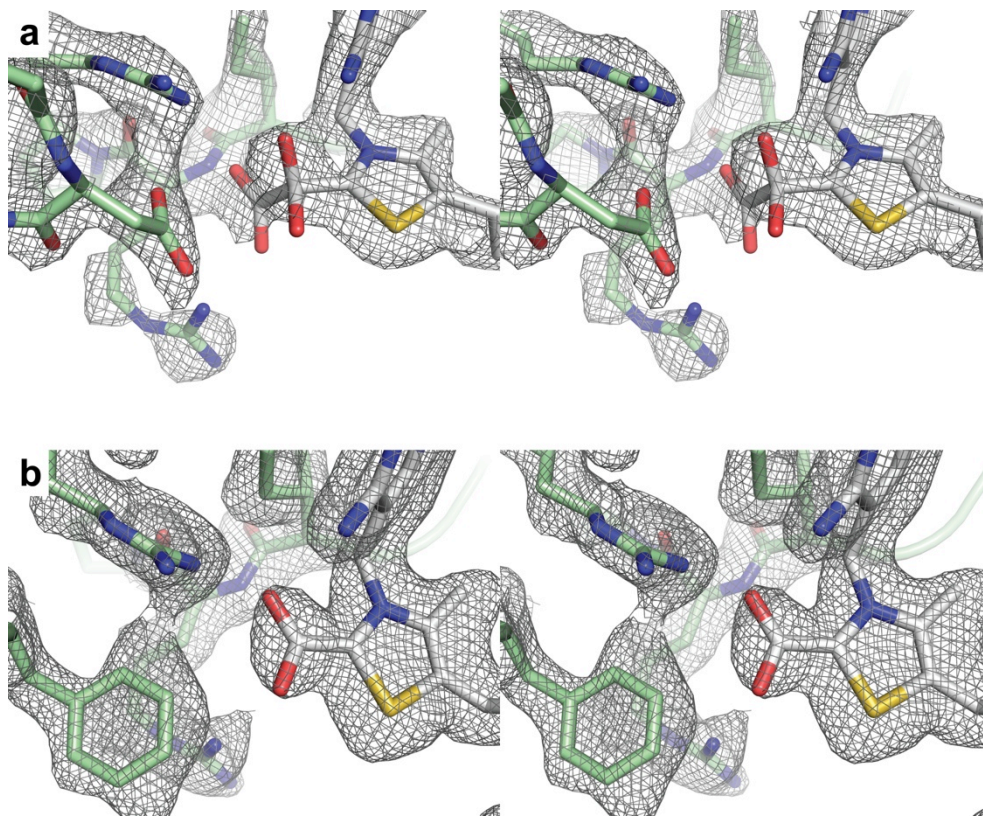


Figure S2. Stereoviews of TPP-bound intermediates shown in Figure 2. **a)** The COOM-TPP intermediate, represented as in Figure 2a. **b)** The carboxy-TPP intermediate, represented as in Figure 2b.

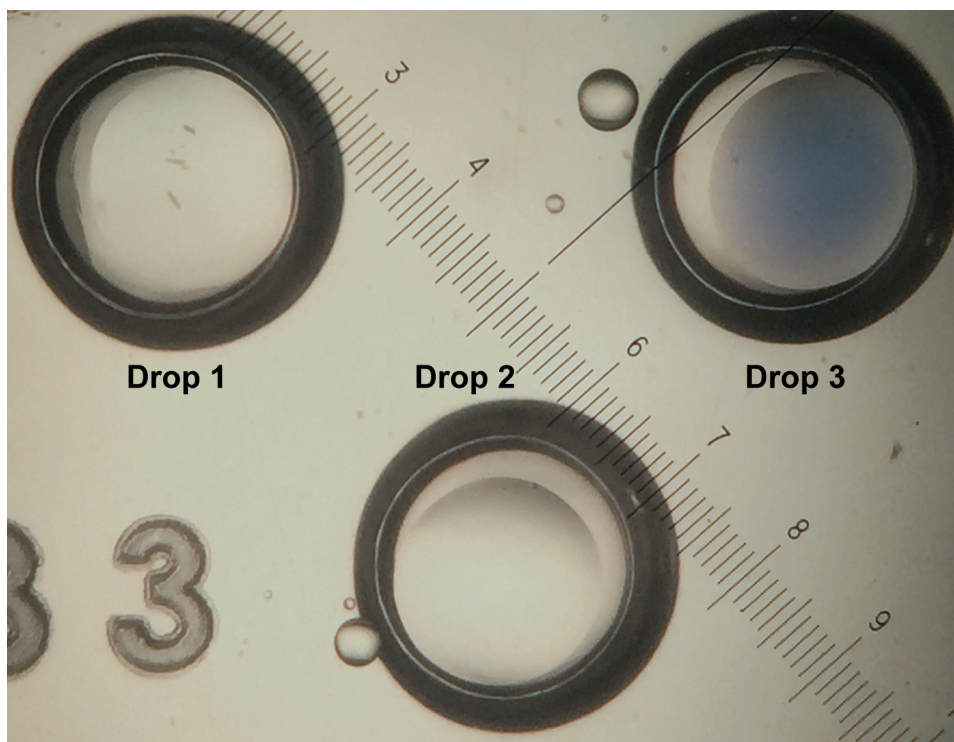


Figure S3. OOR retains activity after crystallization and in the presence of crystallization reagents. Active OOR will oxidize oxalate, reducing methylviologen, and thereby changing the color of methylviologen to blue. OOR crystals were grown as described in the absence of oxalate (3). **Drop 1)** Negative control drop (no oxalate) containing 10 mM oxidized methylviologen and crystallization reagents. Four OOR crystals were washed and soaked in this drop for 24 hours with no color change observed. **Drop 2)** Negative control drop (no crystals) containing 10 mM oxidized methylviologen and 10 mM oxalate pH 8.0. No color change was observed after 24 hours. **Drop 3)** OOR crystal assay drop containing 10 mM oxidized methylviologen and 10 mM oxalate pH 8.0. Four OOR crystals were washed and soaked in this drop for 24 hours, after which the drop was observed to have turned blue, consistent with methylviologen reduction. OOR crystals dissolved over time. The color change was visible by the naked eye; this photograph has had a cooling filter applied evenly across the whole picture to remove the yellow bias created by the microscope through which the picture was taken.

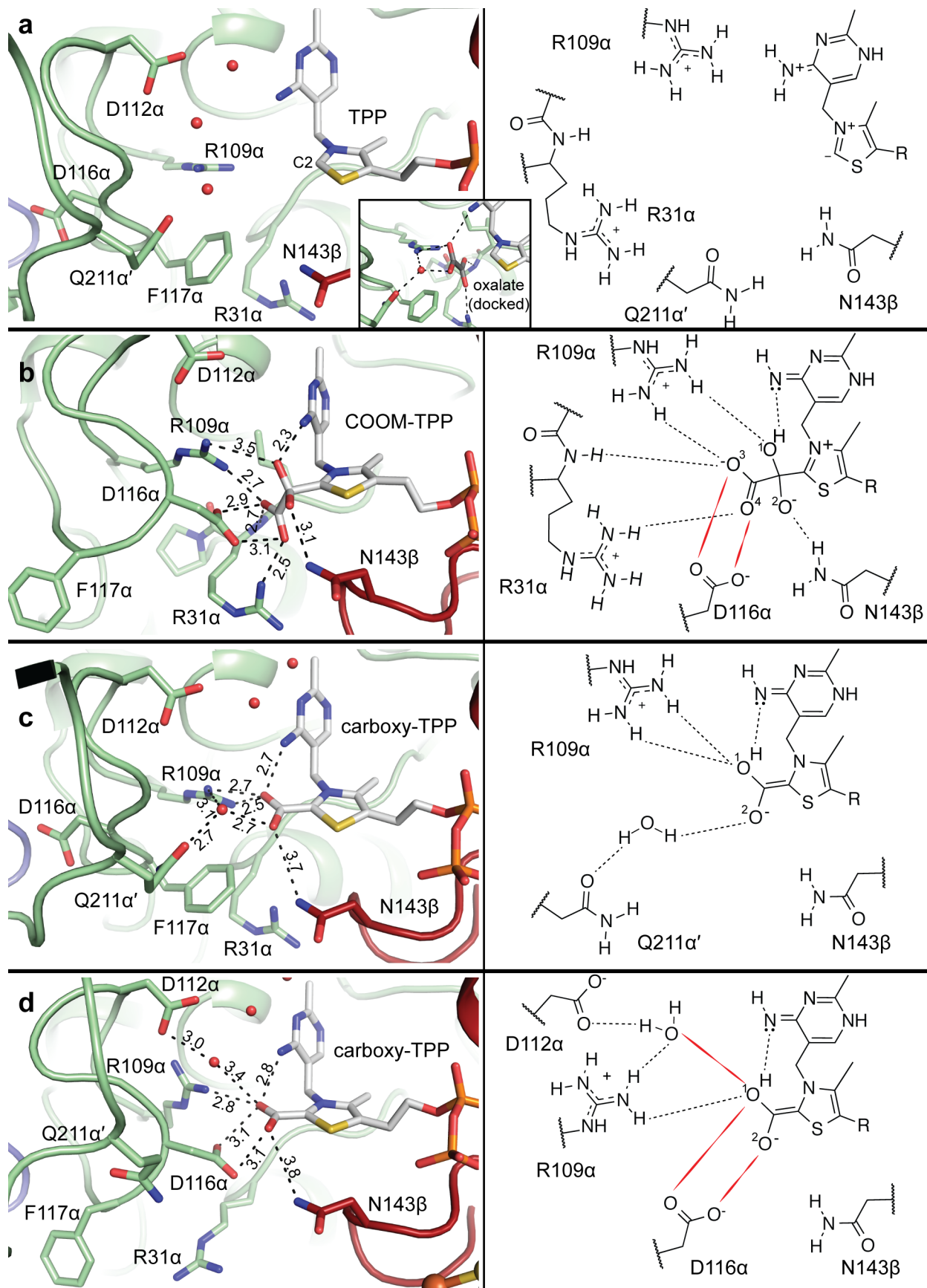


Figure S4. Views of the OOR active site at different stages of catalysis, with corresponding schematics at right. **a)** The active site of as-isolated OOR (PDB ID: 5C4I) (3), is vacant and ready for substrate binding, with the Switch loop in the Asp116 α -out conformation. The inset shows a model of oxalate (with carbons colored dark gray) docked into the substrate binding pocket based on a structure of PFOR with pyruvate (15). **b)** The COOM-TPP intermediate from monomer 2 of the oxalate-soaked crystal is shown with the Switch loop in the Asp-in position. **c)** carboxy-TPP is shown from monomer 1 of the oxalate co-crystal, with the Asp-out loop conformation. Gln211 α' is oriented in toward the active site, forming a hydrogen bond through water to the adduct. **d)** The active site of monomer 2 of the oxalate co-crystal is shown with carboxy-TPP interacting with Asp116 α from the Switch loop in the Asp-in conformation. Gln211 α' is pulled away from the active site and is no longer supporting a water molecule in the same position as in c). In the schematic, protonation states are hypothesized, as is the oxidation state of carboxy-TPP, which is depicted in the most reduced state. Oxygen atoms of the intermediates are numbered in the schematic in b-d). In the structure figures, the protein is shown in ribbon diagram with domain I colored green, domain VI colored red, and TPP adducts colored white. TPP, its adducts, and sidechains of residues Arg31 α , Arg109 α , Asp112 α , Asp116 α , Phe117 α , Gln211 α' , and Asn143 β are shown as sticks. Select active-site water molecules are shown as non-bonded red spheres and dashed lines indicate close distances to TPP bound adducts. In the schematic, potential hydrogen-bonding interactions with bound substrate are indicated by black dashed lines, and interactions that are hypothesized to be charge-repulsion interactions are shown as red contoured lines. The complete structure of TPP is shown in Figure S1A.

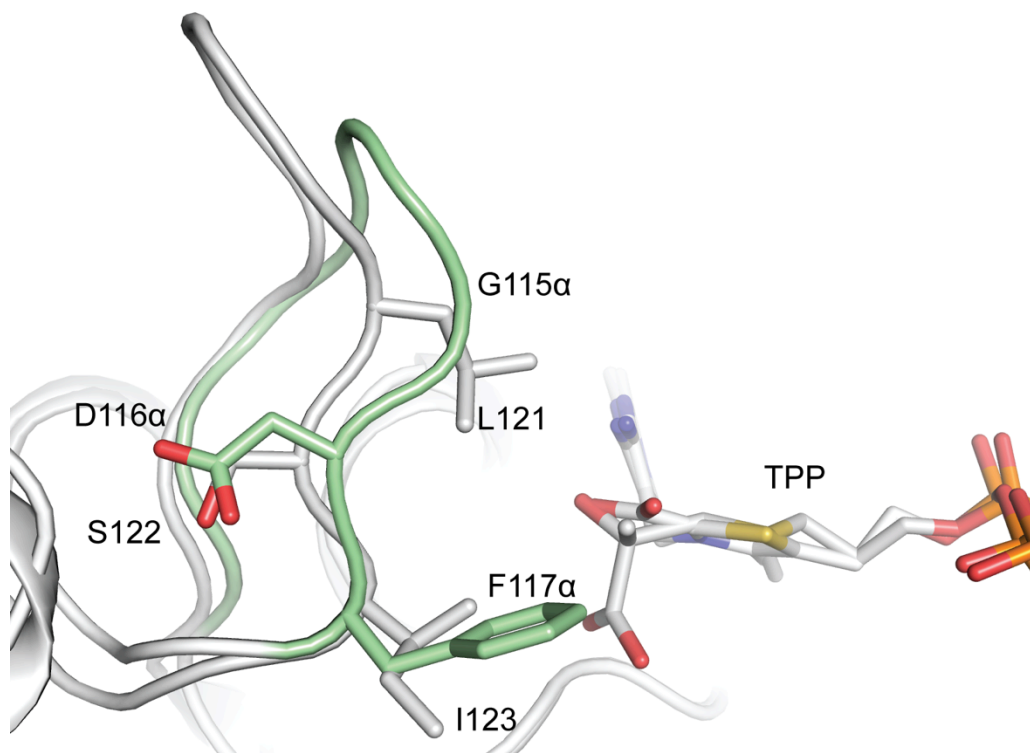


Figure S5. The Asp-out conformation of the OOR Switch loop is analogous to the conformation of the same loop in *Da* PFOR. Domain I from both OOR (monomer 1 of the oxalate co-crystal) and chain A of *Da* PFOR (PDB ID: 2C3P) is shown in ribbon diagram, with the two enzymes overlaid onto each other. The carboxy-TPP intermediate for OOR and the lactyl-TPP intermediate for PFOR are shown as sticks. The Switch loop in OOR is colored green, whereas everything else is colored white. In PFOR, Leu121 and Ile123 form a hydrophobic interaction for the methyl group of pyruvate. In PFOR, Asp116 α and Phe117 α are capable of flipping to bring Asp116 α into contact with the TPP-bound intermediate.

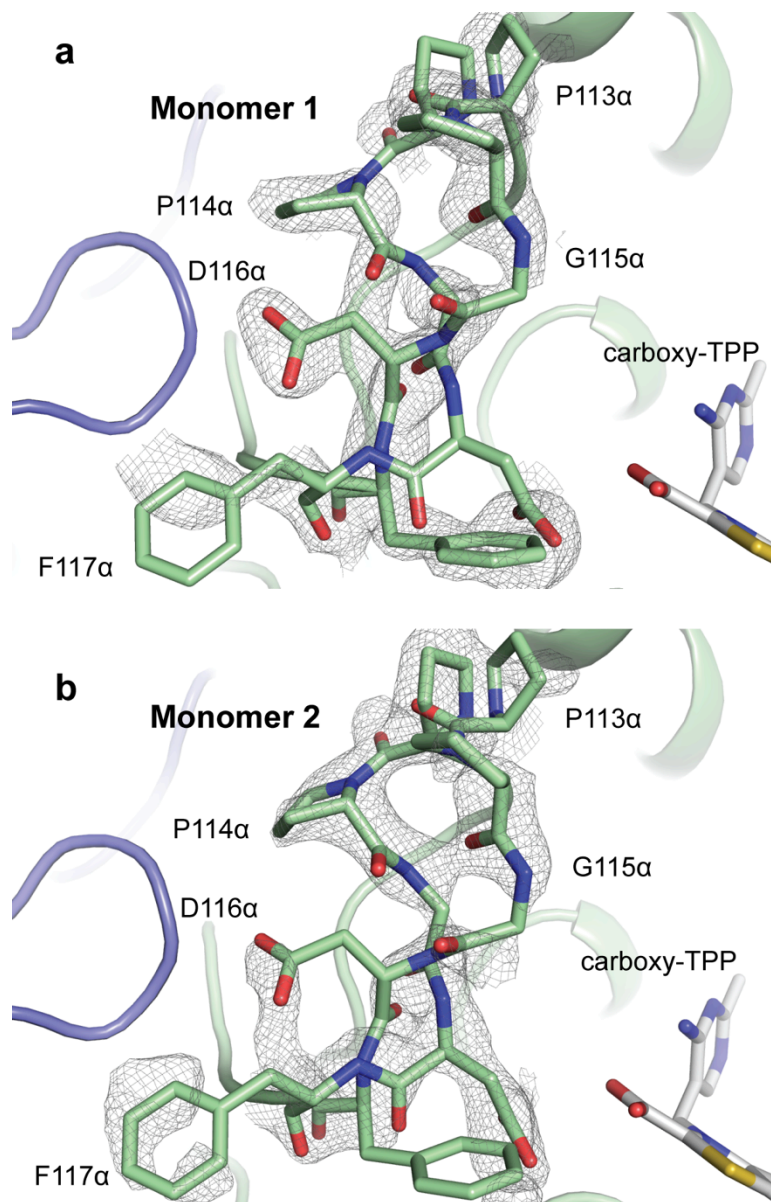


Figure S6. Electron density in the oxalate co-crystal shows that both Switch loop conformations are present at different occupancies. **a)** The Switch loop of monomer 1 is shown in both conformations in stick representation. Simulated-annealing composite-omit maps contoured to 1σ are shown as a gray mesh. The Asp-out conformation is dominant in this monomer (62%), though there is clearly density for the alternate conformation as well. **b)** The Switch loop of monomer 2 with simulated-annealing composite-omit maps shown as in a). Again, density is visible for both loop conformations, though the Asp-in conformation is dominant (58%).

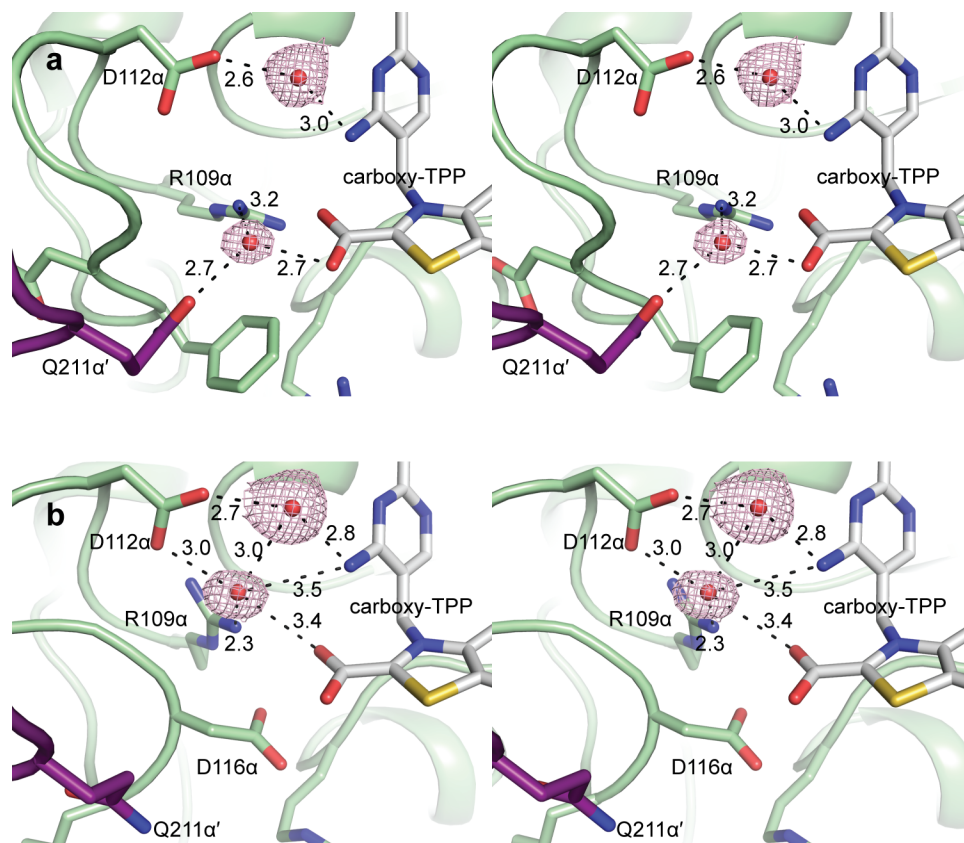


Figure S7. Movement of Gln211 α' and active-site water arrangement is correlated with the conformation of the Switch loop in the oxalate co-crystal structure. **a).** The active site of monomer 1 is shown in stereo. The Switch loop is in the Asp-out conformation, and Gln211 α' is pointed toward the substrate-binding pocket. Active-site residue side chains and the carboxy-TPP intermediate are depicted as sticks and waters as non-bonded spheres. Simulated-annealing composite-omit density is shown in pink mesh around the water molecules. Contacts within hydrogen bonding distance to the water molecules are indicated with dashed lines, with distances given. Residues making contacts to the depicted waters are labeled. **b).** The active site of monomer 2 is shown as in a). The Switch loop is in the Asp-in conformation and Gln211 α' is pulled away from the active site.

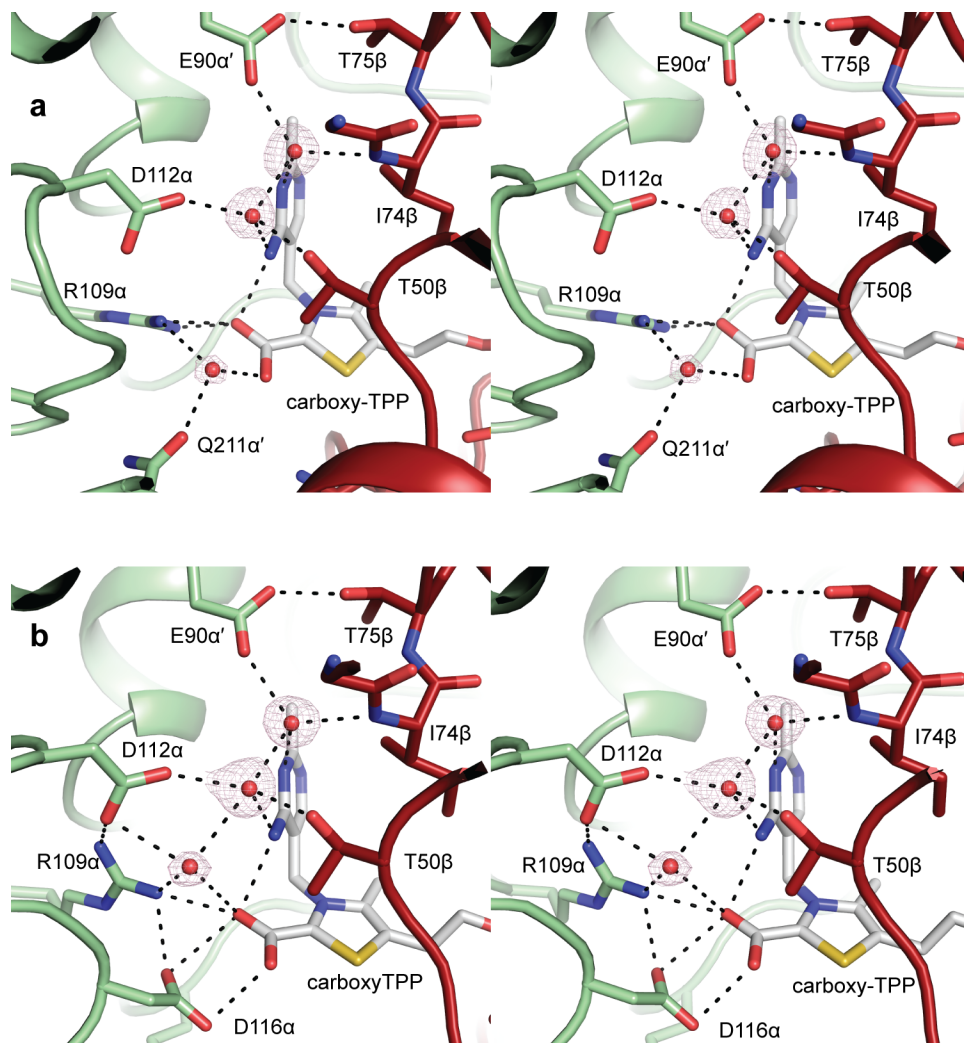


Figure S8. Stereoviews of the extended hydrogen-bonding networks in the oxalate co-crystal. **a)** The active site of monomer 1 is shown with carboxy-TPP and residue side chains shown as sticks, waters shown as non-bonded spheres, and composite-omit maps around the waters as a pink mesh at 1.5 σ cutoff. Relevant interactions indicated with dashes. **b)** The active site of monomer 2 is shown in the same manner as a). The water that interacts with Gln211 α' in a) moves up to interact with Asp112 α in b) to join a water network up through the active site.

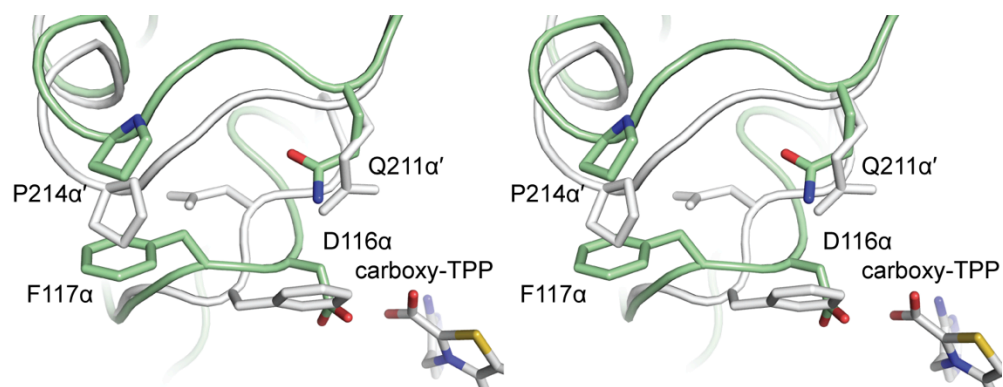


Figure S9. Stereoview of loop movement in the active site of monomer 2 of the oxalate co-crystal. Alternate conformations of loops containing residues 113-118 of chain α and residues 210-220 of chain α' are shown, with noted active-site residues shown in sticks. Residues belonging to the Asp-in conformation are shown in green with colored heteroatoms, whereas residues in the Asp-out conformation are colored white. In the Asp-in conformation, Phe117 α interacts with Pro214 α' , pushing it up and away from the active site. At the same time, Asp116 α blocks Gln211 α' , and directs it away from the active site.

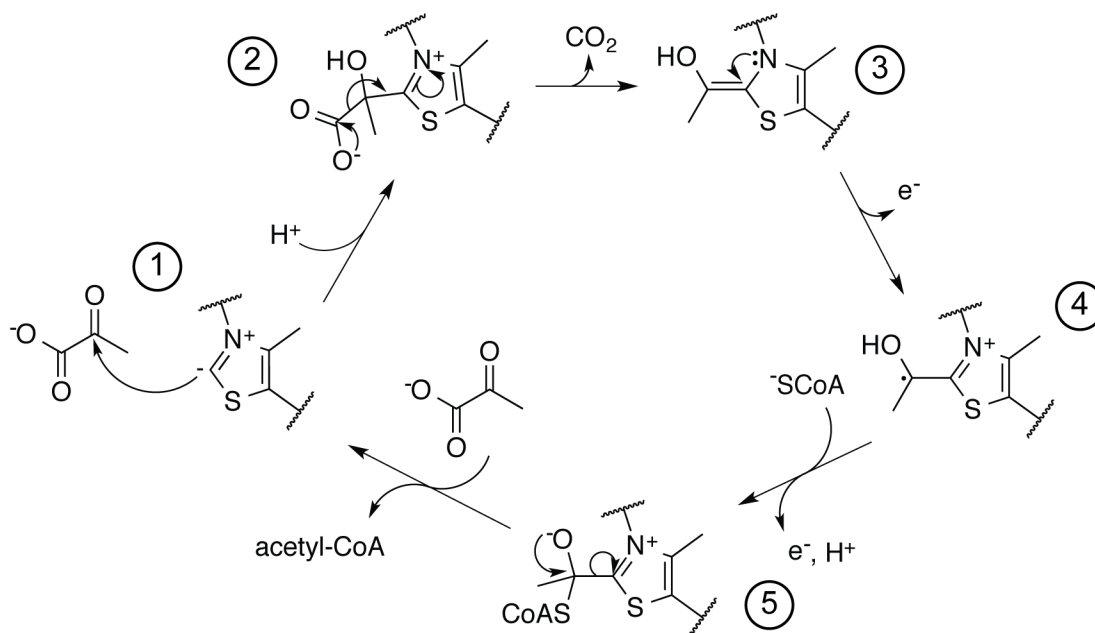


Figure S10. The mechanism of pyruvate oxidation by PFOR, based on that proposed by Reed et al. (16). TPP initiates catalysis by nucleophilic attack on the carbonyl group of pyruvate (state 1), forming a lactyl-TPP intermediate (state 2). This intermediate undergoes decarboxylation (state 3) and one-electron oxidation to form the so-called hydroxyethylidene-TPP (HE-TPP) intermediate (state 4), here shown protonated, though in solution studies this species appears to exist in an equilibrium of protonation states (16). Nucleophilic attack by CoA drives the second oxidation step (state 5) following which acetyl-CoA is eliminated as the product, regenerating the TPP catalytic cofactor.

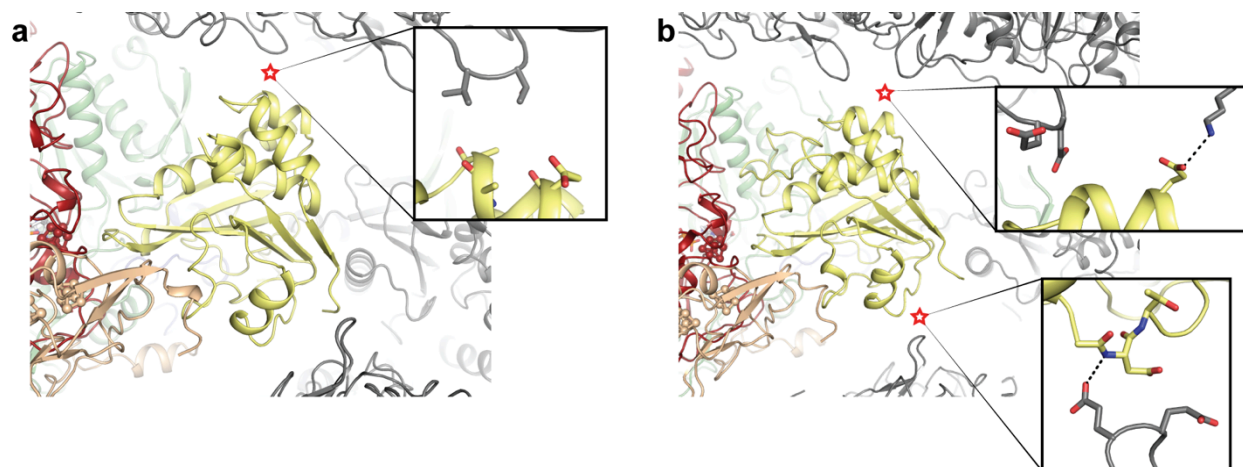


Figure S11. Lattice contacts can stabilize domain III (yellow) in either the “out” position or the “in” position. **a)** In monomer 1 of the oxalate-soaked crystal, domain III is stabilized by lattice contacts in the “out” position, the plug loop is disordered, and electron density was not consistent with a specific adduct, likely representing a mixture of adduct-bound states. Monomer 1 is colored by domain, whereas other molecules in the unit cell are colored dark gray. The red star indicates the lattice contact, which is depicted in greater detail in the inset. **b)** In monomer 2, lattice contacts prohibit domain III from rotating out from the active site, and the electron density is consistent with oxalate being present in the active site. The red stars indicate lattice contacts, which are depicted in greater detail, including potential hydrogen-bonding interactions, in the insets.

Supporting Tables

Supporting Table 1. Data Collection and Model Refinement Statistics

	OOR-oxalate soak	OOR-oxalate co-crystal
Data collection and processing		
Space group	$P4_3$	$P2_12_12_1$
Cell dimensions (Å)	$a = b = 138.4, c = 217.1$	$a = 113.6, b = 144.1, c = 161.7$
Wavelength (Å)	0.97900	0.97920
Resolution (Å)	50-2.50 (2.54-2.50)*	50-1.88 (1.91 – 1.88)
Total unique reflections	131,805	200,377
Completeness (%)	93.2 (64.5)	94.4 (75.0)
Redundancy	4.7 (3.4)	5.9 (4.1)
$\langle I/\sigma \rangle$	6.8 (1.9)	7.7 (1.9)
Rsym [†] (%)	18.3 (64.1)	12.9 (88.2)
CC _{1/2} (%)	(85.0)	(86.7)
Model Refinement		
R-work (%)	19.6	17.7
R-free (%)	22.9	20.7
Protein atoms	30,365	17,975
TPP-Mg ²⁺ atoms	108	54
Oxalate adduct atoms	6	-
CO ₂ adduct atoms	-	6
[4Fe-4S] atoms	96	48
Solvent atoms	17	2,225
RMS(bonds) (Å)	0.003	0.007
RMS(angles) (°)	0.707	1.003
Ramachandran favored (%)	96.8	97.0
Ramachandran allowed (%)	3.0	2.9
Ramachandran outliers (%)	0.2	0.1
Average <i>B</i> -factor (Å ²)	36.0	28.8
Protein (Å ²)	36.1	27.4
TPP-Mg ²⁺ (Å ²)	28.0	19.2
Oxalate adduct (Å ²)	31.4	-
CO ₂ adduct (Å ²)	-	24.4
[4Fe-4S] (Å ²)	32.8	20.1
Solvent (Å ²)	26.8	40.9

* Numbers in parenthesis indicate the highest resolution bin.

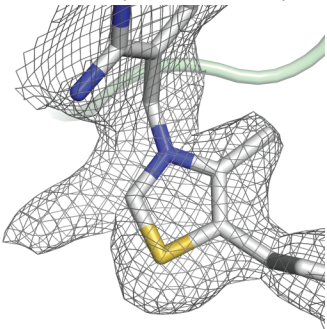
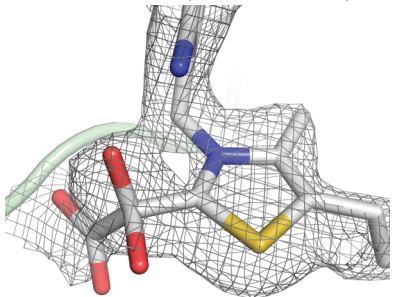
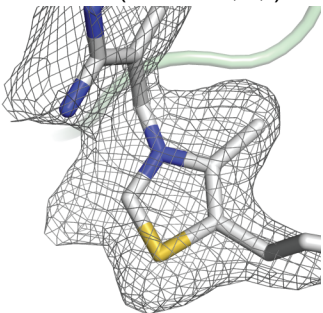
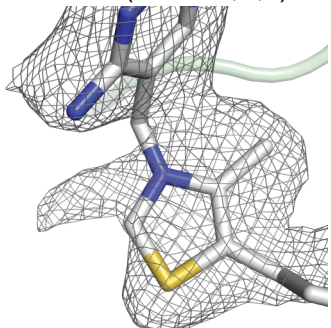
[†] $\sum(|I - \langle I \rangle|) / \sum(I)$

Supporting Table 2. Model completeness* of OOR crystal structures.

	OOO-oxalate soak	OOO-oxalate co-crystal
Chain	Omitted Residues	
A	1	1
B	1-3, 146-164, 211-217	1-2, 214-217
C	313-314	-
D	1	1
E	1-5, 40-43, 211-221	1, 146-164, 214-218
F	311-314	314
G	1	N/A
H	1-4, 145-164	N/A
I	310-314	N/A
J	1	N/A
K	1-5, 145-165, 210-218	N/A
L	311-314	N/A
Chain	Residues modeled as alanine	
A	3, 284	3
B	4, 29, 145, 191, 226	-
C	-	-
D	233, 261, 314, 383	383
E	13, 15, 29, 69, 103, 116, 135, 143, 145, 174, 186, 196, 208, 314	4, 26, 145, 176, 314
F	266, 267, 279	-
G	3, 233, 383	N/A
H	5, 6, 29, 50, 191	N/A
I	1, 4, 267	N/A
J	3, 31, 383	N/A
K	26, 29, 101, 103, 116, 118, 119, 123, 174, 176, 180, 227, 314	N/A
L	38, 264	N/A
Chain	Residues modeled in two conformations (oxalate co-crystal only)	
A	-	31, 108-119, 210-220
B	-	-
C	-	-
D	-	31, 108-119, 210-220
E	-	-
F	-	-

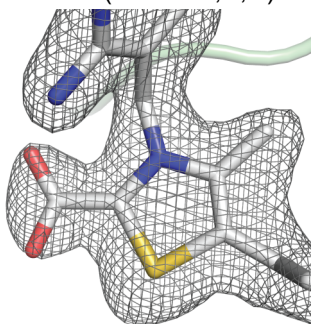
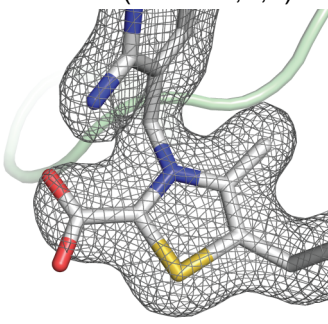
*Chains A, D, G, J have 395 residues. Chains B, E, H, K have 315 residues. Chains C, F, I, L have 314 residues.

Supporting Table 3. Features of the different monomers in the asymmetric unit of the oxalate-soaked OOR crystal.*

Space Group	$P4_3$ (twinned)	
Resolution	2.50 Å	
Storage Buffer	50 mM Tris, pH 8.0, 2 mM DTT	
Drop conditions	$\frac{1}{2}$ protein (in storage buffer) + 4-5 % PEG 3,000, 1-2% Tacsimate	
Cryo conditions	Drop conditions + 20% PEG 400 + 10 mM oxalate pH 8.0 (1-5 minutes)	
Active Site	Monomer 1 (chains A,B,C)	Monomer 2 (chains D,E,F)
Active-site omit density ($1\ \sigma$)		
Intermediate, occupancy	TPP; (Disordered density with nothing modeled)	Carboxy-dioxidomethyl (COOM)-TPP, 89%
Switch loop	Asp-in	Asp-in
Domain III loop	Disordered	Ordered
Domain III crystal contacts	Contacts stabilizing the <i>in</i> position of domain III	Contacts stabilizing the <i>out</i> position of domain III
Active Site	Monomer 3 (chains G,H,I)	Monomer 4 (chains J,K,L)
Active-site omit density ($1\ \sigma$)		
Intermediate	TPP; (Disordered density with nothing modeled)	TPP; (Disordered density with nothing modeled)
Switch loop	Asp-in	Asp-in
Domain III loop	Disordered	Disordered
Domain III crystal contacts	Contacts stabilizing the <i>out</i> position of domain III	Not many close contacts

*See text for definitions of “Switch loop,” “Domain III loop,” and “Domain III crystal contacts.”

Supporting Table 4. Features of the different monomers in the asymmetric unit of the oxalate co-crystal.

Space Group	$P2_12_12_1$	
Resolution	1.88 Å	
Storage Buffer	50 mM Tris, pH 8.0, 2 mM DTT	
Drop conditions	$\frac{1}{2}$ protein (in storage buffer) + 4-5 % PEG 3,000, 1-2% Tacsimate + 10 mM oxalate	
Cryo conditions	Drop conditions + 20% PEG 400 (1-5 minutes)	
Active Site	Monomer 1 (chains A,B,C)	Monomer 2 (chains D,E,F)
Active-site omit density (1σ)		
Intermediate, occupancy	Carboxy-TPP (best density), 61%	Carboxy-TPP, 65%
Switch loop	Asp-out	Asp-in
Domain III loop	Ordered	Disordered
Domain III crystal contacts	No contacts	No contacts

*See text for definitions of "Switch loop," "Domain III loop," and "Domain III crystal contacts."

References

1. Pierce E, Becker DF, Ragsdale SW (2010) Identification and Characterization of Oxalate Oxidoreductase, a Novel Thiamine Pyrophosphate-dependent 2-Oxoacid Oxidoreductase That Enables Anaerobic Growth on Oxalate. *J Biol Chem* 285(52):40515–40524.
2. Elliott JI, Brewer JM (1978) The inactivation of yeast enolase by 2,3-butanedione. *Arch Biochem Biophys* 190(1):351–357.
3. Gibson MI, et al. (2015) The Structure of an Oxalate Oxidoreductase Provides Insight into Microbial 2-Oxoacid Metabolism. *Biochemistry* 54(26):4112–4120.
4. Otwinowski Z, Minor W (1997) Processing of X-ray Diffraction Data Collected in Oscillation Mode. *Macromolecular Crystallography, Part A, Methods in Enzymology.*, eds Carter CW Jr, Sweet RM (Academic Press, New York), pp 307–326.
5. Zwart PH, Grosse-Kunstleve RW, Adams PD (2005) Characterization of X-ray data sets. *CCP4 Newsl* (42).
6. Zwart PH, Grosse-Kunstleve RW, Adams PD (2005) Xtriage and Fest: automatic assessment of X-ray data and substructure structure factor estimation. *CCP4 Newsl* (43).

7. Adams PD, et al. (2010) *PHENIX*: a comprehensive Python-based system for macromolecular structure solution. *Acta Crystallogr D Biol Crystallogr* 66(2):213–221.
8. McCoy AJ, et al. (2007) *Phaser* crystallographic software. *J Appl Crystallogr* 40(4):658–674.
9. Emsley P, Lohkamp B, Scott WG, Cowtan K (2010) Features and development of *Coot*. *Acta Crystallogr D Biol Crystallogr* 66(4):486–501.
10. Frisch MJ, et al. (2004) *Gaussian 03, Revision D01* (Gaussian, Inc., Wallingford, CT).
11. Lee C, Yang W, Parr RG (1988) Development of the Colle-Salvetti correlation-energy formula into a functional of the electron density. *Phys Rev B Condens Matter* 37(2):785–789.
12. Becke AD (1993) Density-functional thermochemistry. III. The role of exact exchange. *J Chem Phys* 98(7):5648–5652.
13. Hariharan PC, Pople JA (1973) The influence of polarization functions on molecular orbital hydrogenation energies. *Theor Chim Acta* 28(3):213–222.
14. Kung Y, Doukov TI, Seravalli J, Ragsdale SW, Drennan CL (2009) Crystallographic Snapshots of Cyanide- and Water-Bound C-Clusters from Bifunctional Carbon Monoxide Dehydrogenase/Acetyl-CoA Synthase. *Biochemistry* 48(31):7432–7440.
15. Cavazza C, et al. (2006) Flexibility of Thiamine Diphosphate Revealed by Kinetic Crystallographic Studies of the Reaction of Pyruvate-Ferredoxin Oxidoreductase with Pyruvate. *Structure* 14(2):217–224.
16. Reed GH, Ragsdale SW, Mansoorabadi SO (2012) Radical reactions of thiamin pyrophosphate in 2-oxoacid oxidoreductases. *Biochim Biophys Acta BBA - Proteins Proteomics* 1824(11):1291–1298.